This article has been accepted for publication in a future issue of this journal, but has not been fully edited. Content may change prior to final publication. Citation information: DOI 10.1109/LAWP.2020.3022520, IEEE Antennas and Wireless Propagation Letters

High-Gain Millimeter-Wave Holographic Antenna in Package using Glass Technology

Thomas Galler, *Student Member, IEEE,* Thomas Frey, *Student Member, IEEE,*
Christian Waldschmidt, *Senior Member, IEEE,* and Tobias Chaloun, *Member, IEEE,*

***Abstract*—A novel concept for a holographic antenna-in-package (AiP) is presented enabling the seamless integration of high gain antennas at millimeter wave frequencies. The antenna is based on a holographic impedance approach stimulating a leaky wave mode at 150 GHz. Since the antenna structure is placed on top of the glass package, a large antenna aperture with high angular beam width and efficiency were achieved. The surface wave launcher (SWL) of the antenna connected to the integrated active circuitry is designed in a very compact fashion using a vertical through-glass-via (TGV) and solder balls. The performance of the proposed holographic antenna package has been investigated by an analytic model and full wave simulations. The measurement results of the antenna prototype on glass using anisotropic unit cells show excellent agreement to the simulated values. A maximum gain of 24.7 dBi, a sidelobe level of 15 dB, and a 3 dB-beam width of 4.7° are achieved. The measured 3D-radiation pattern shows a highly directive pattern in all cuts.**

***Index Terms*—holographic, antenna, glass, TGV, hermetically sealed, package.**

I. Introduction

Developments in silicon-germanium (SiGe) technology nowadays enable the integration of fully transceiver circuits into miniaturized sensor systems [1]. Frequencies above 100 GHz provide large absolute bandwidths leading to high range resolution. However, there is still a lack of high gain antennas for high angular resolution radar front ends. Antenna arrays at millimeter-wave frequency using a planar distribution network suffer from high losses [2] or a large size. In addition, antenna integration on monolithic microwave integrated circuits (MMICs) results in a large chip area and cost effective production as antenna and chip size are connected. Integrated antenna on chip (AoC) solutions [3], [4] show typically a poor radiation efficiency due to the high permittivity and high losses of the semiconductor configuration.

One approach to overcome these drawbacks is to implement the antenna into the package (AiP) [5]. This allows a more scalable antenna size with more flexibility with respect to the antenna position. The disadvantage of such a system is the use of a more complex feeding network to connect the antenna with the MMIC. Antenna on chip (AoC) solutions suffer from a non efficient distribution network which results in a small aperture and therefore a large beam width. A second solution is to integrate the antenna on chip (AoC) as a primary feed illuminating a dielectric lens to enhance the gain and beam width [6]. However, the sensor package becomes more bulky, and additional alignment of the antenna towards the lens is necessary. In this paper, a novel packaging concept for frequencies beyond 150 GHz is presented combining the features of glass material and holographic antenna topology [7]. This efficient approach enables large physical antenna apertures with low fabrication tolerances and low cost material at the same time. A linearly or circularly polarized leaky wave (LW) radiation is generated due to the impedance hologram of spiral pixel structures [8].

This work was funded by the VDI/VDE Innovation + Technik GmbH within the project GlaRA. – 16ES0692 (Corresponding author: Thomas Galler)

The authors are with the Institute of Microwave Engineering, Ulm University, 89081 Ulm, Germany e-mail: thomas.galler@uni-ulm.de.

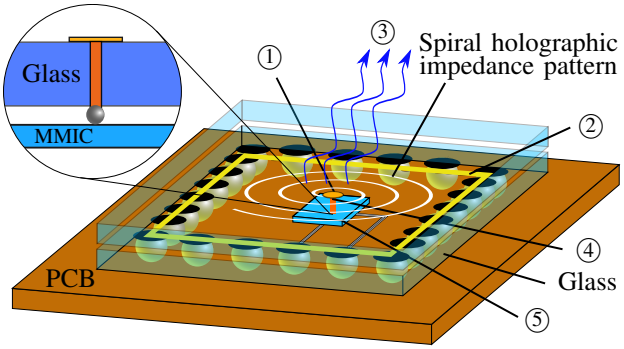

Fig. 1: Perspective view of the proposed holographic antenna-in-package using glass: ① surface wave launcher, ② seal ring, ③ leaky wave, ④ through-glass-via, ⑤ MMIC

II. Packaging Concept

The proposed holographic antenna-in-package (AiP) architecture for millimeter-wave sensory systems is illustrated in Fig. 1. The package consists of two glass layers in which a radar MMIC is hermetically sealed [9]. In the upper glass layer the RF signal is guided from the packaged MMIC to the antenna by solder ball interconnections and a vertical TGV (Fig. 1). Due to the galvanic plated TGV and the seal ring between the glass layers, this results in a hermetically sealed chip package.

III. Surface wave Launcher

The fundamental TM_0 surface wave is excited by a circular patch placed on top of the upper glass layer (see Fig. 1). According to the cylindrical geometry electromagnetic field components are rotationally symmetric as shown in Fig. 2b. A TGV connects the patch with the CPW line on the bottom side

This article has been accepted for publication in a future issue of this journal, but has not been fully edited. Content may change prior to final publication. Citation information: DOI 10.1109/LAWP.2020.3022520, IEEE Antennas and Wireless Propagation Letters

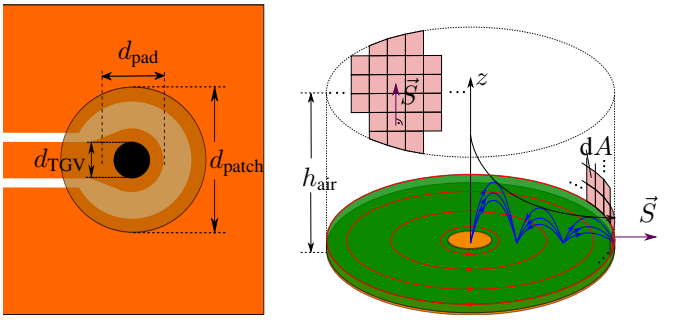

(a) Top and side view of the surface-wave launcher on glass

(b) Perspective view of the simulation model

Fig. 2: Design of a compact surface wave launcher on glass.

of the glass. This feeding method results in a very compact and simple antenna configuration compared to primary end fire exciters. In order to quantify the surface wave launcher on glass a novel optimization methodology is proposed:

$$P_{\text{wall}} = \oiint_{A_{\text{wall}}} \left|\vec{S}\right| \mathrm{d}A = \frac{1}{2} \oiint_{A_{\text{wall}}} \left(E_z H_y^* - E_z H_x^*\right) \mathrm{d}A. \quad (1)$$

In order to quantify the effective power transformed in the SW mode an integration of the pointing vector $\vec{S}$ is done as shown in Fig. 2b. The surface wave coupling ratio η_{SW} reads as the power bound on the surface (P_{wall}) divided by the total transmitted power P_{top}, P_{wall} and losses P_{loss}:

$$\eta_{\text{SW}} = \frac{P_{\text{wall}}}{P_{\text{top}} + P_{\text{wall}} + P_{\text{loss}}}. \quad (2)$$

The parametric study and optimization of the surface wave launcher have been carried out using a full wave simulation tool [10]. Fig. 3 shows the efficiency for different frequencies with a maximum value of 0.92. The prototype is realized

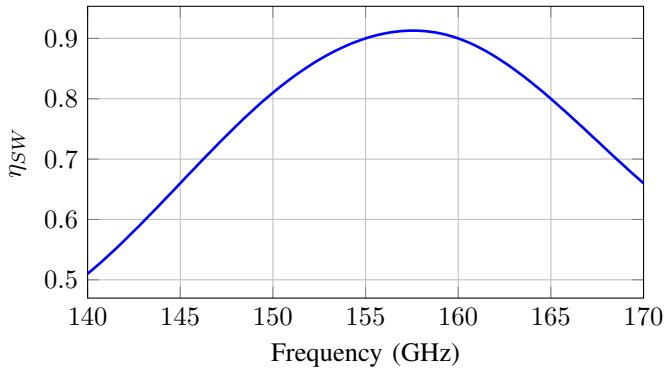

Fig. 3: Efficiency of SWL with d_{patch}=1120 µm and d_{TGV}=44 µm.

in fused silica with a thickness of 160 µm, which offers mode purity of the fundamental TM_0 mode. Fused silica is characterized with permittivity $\varepsilon_r = 3.78$ and dielectric loss $\tan\delta = 0.001$ at 150 GHz. The connecting TGV is formed by a laser-induced-deep-etching process (LIDE) from LPKF [11] and a subsequent metalization step for galvanic plating. Using this approach aspect ratios beyond 1:10 are possible.

IV. Synthesis of the Holographic Antenna

The proposed design process (cf.Fig. 4) for holographic antennas is based on an analytic antenna design process [12],[13]. In order to radiate leaky waves, a planar surface wave (SW) needs to be stimulated as a point source. It interacts with a subwavelength periodic surface structure of discontinuities. The fundamental TM_0 SW mode is excited by a SWL, which is discussed in section III. Its transversal magnetic field distribution $\vec{H}_t(x,y)$ and electric field distribution $\vec{E}_t(x,y)$ on the antenna aperture located at $z = 0^+$ are given by [14]. For the calculation of the transversal electric field an impedance boundary condition (IBC) is defined, where the impedance tensor $\overleftrightarrow{Z}$ could have an isotropic or anisotropic form. Assuming the electric objective field possesses the form (see ① in Fig. 4)

$$\vec{E}_{\text{obj}}(x,y)\,|_{z=0^+} = \begin{pmatrix} |E_{x_0}|\,\mathrm{e}^{-\mathrm{j}(k_x x)} \\ |E_{y_0}|\,\mathrm{e}^{-\mathrm{j}\left(k_y y \mp \frac{\pi}{2}\right)} \end{pmatrix} \begin{pmatrix} T_x(x,y) \\ T_y(x,y) \end{pmatrix}, \quad (3)$$

where T_x and T_y are the x- and y-components of an desired amplitude taper function $T(x,y)$, E_{x_0} and E_{y_0} are real space-independent amplitudes, and the complex expression corresponds to the space-dependent phase, which equals the inphase and the quadrature term to generate a circular polarization. A weakly radiative objective field, according to [12], needs to be added for a pure reaktive impedance tensor. This leads to the definition of the impedance tensor (see ③ in Fig. 4), where Z_{avg} is the offset value of the impedance modulation. Projecting (4) along its x- and y-polarization the TM- and TE-components of the impedance tensor are obtained:

$$\overleftrightarrow{Z} \begin{pmatrix} \cos(\phi) \\ \sin(\phi) \end{pmatrix} = Z_{\text{avg}} \begin{pmatrix} \cos(\phi) \\ \sin(\phi) \end{pmatrix} + 2 \cdot \mathrm{Im}\left\{ \frac{\vec{E}_A}{I_{\text{TM}_0} H_1^{(2)}} \right\}. \quad (4)$$

The space-dependent modulation indices allow a synthetization of the amplitude distribution from the

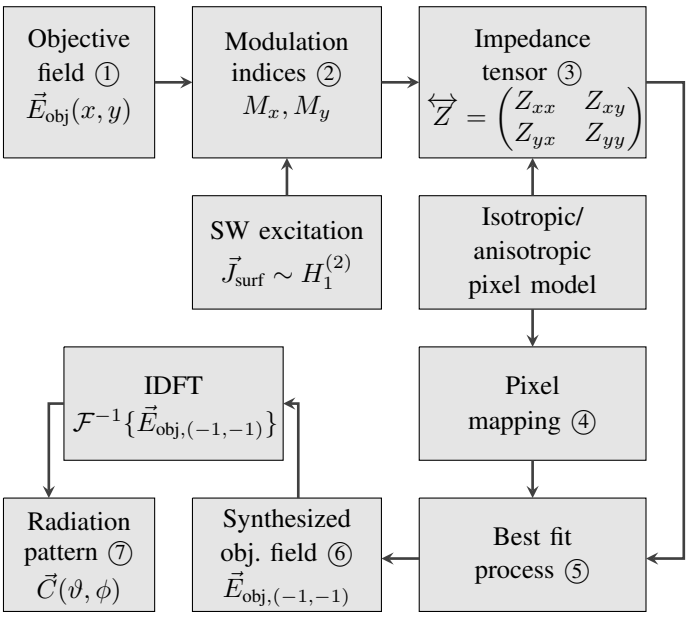

Fig. 4: Design process of the analytical antenna model.

This article has been accepted for publication in a future issue of this journal, but has not been fully edited. Content may change prior to final publication. Citation information: DOI 10.1109/LAWP.2020.3022520, IEEE Antennas and Wireless Propagation Letters

desired electric aperture field (see ① in Fig. 4). The synthesized objective field (see ⑥ in Fig. 4) equals the electric field distribution of the (−1,−1)-LW mode, whose Fourier spectrum is related to the far field pattern of the holographic antenna (see ⑦ in Fig. 4). Hence, the control of the modulation indices allows a specified configuration of the far field pattern in relation to the side lobe level and the main beam width. It can be calculated as follows (see ② in Fig. 4):

$$M_x(x,y) = \left| \frac{\vec{E}_{\text{obj},x}(x,y)}{\vec{E}_{\text{t,avg}}} \right| \quad M_y(x,y) = \left| \frac{\vec{E}_{\text{obj,y}}(x,y)}{\vec{E}_{\text{t,avg}}} \right|. \quad (5)$$

Furthermore, a beam steering is possible due to the phase information of the tensor components. Finally, an analytical synthesis of a desired aperture field and its far field pattern are done as illustrated in Fig. 4.

V. Pixel Modelling

The theoretical impedance hologram can be obtained from the analytic antenna model from section IV. For the realization of these surface impedances a pixel modelling is necessary (see ④ in Fig. 4). The unit cell (UC) dimensions need to be small compared to the wavelength to get an homogeneous periodic structure. The variation of the impedance is achieved by changing the geometrical parameters of the pixel, which is located in the center of the unit cell. In order to enhance the co- to cross-polarisation isolation, an anisotropic impedance tensor is necessary. Therefore, the pixel geometry has an additional feature to realize that anisotropic impedance tensor, which converts the fundamental SW mode in a TM-TE-hybrid leaky wave mode. A method for the tensor realization and controlling the coupling between currents in every direction is inserting a slot [13] through the center of the pixel, where the slot has an orientation angle and a gap width (see Fig. 5). The impenetrable surface wave impedance can be obtained by solving the eigenmode problem of the unit cell. As a result, only eigenmodes fulfilling the periodic boundary conditions, are able to propagate. These eigenmodes have a valid solution for the eigenfrequency ω_0 and its corresponding effective wavenumber k_{SW}. Its real part corresponds to the phase constant of the TM_0 surface wave. The scalar surface impedance depends on the pixel geometry is given by

$$Z_{\text{surf}}^{\text{TM/TE}} = \text{j}Z_{F0}\sqrt{\left(\frac{\beta_{\text{SW}}}{k_0}\right)^2 - 1}. \quad (6)$$

This impedance and the corresponding geometrical values are stored in a database. Out of the analytical antenna model results an impedance tensor for each unit cell, a complex eigenvalue problem depending on the propagation angle of the surface wave has to be solved. Subsequently, a best fit algorithm optimizes each pixel to assign the pixel geometry to each analytical impedance tensor (see ⑤ in Fig. 4). For the realization of this impedance hologram and to ensure an homogeneous periodic structure, a unit cell size of $0.2\,\text{mm} \times 0.2\,\text{mm}$ is used.

VI. Realization and Measurement

In order to characterize the proposed holographic antenna on glass, a prototype has been realized. In Fig. 5, the schematic cross section of the glass antenna is presented.

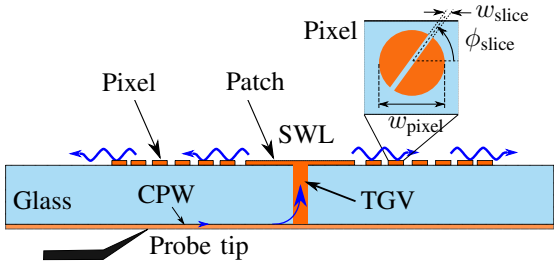

Fig. 5: Cross section of the proposed holographic antenna.

Here, a probe tip in upside-down orientation is used to feed the proposed holographic antenna (see Fig. 7) on glass from the bottom side in order to avoid parasitic impact of the probe on the radiation pattern of the antenna under test. A coplanar line embedded in the ground metalization is used to feed the SWL and allows the direct probing without an extra transition. The dimensions of the CPW feeding correspond to the characteristic impedance of 50 Ω. The metalization consists of chromium with a thickness of 100 nm as a seed layer and subsequent sputtered gold with a thickness of 400 nm. 28900 circular pixels resulting in an aperture of 35 mm × 35 mm, are structured on the antenna surface. The maximum range of the impedance modulation is defined by the modulation index, which is set to $\max\{M_{x,y}\} = 0.3$ and the average impedance equals $Z_{\text{avg}} = \text{j}262\,\Omega$. The top and bottom view of the fabricated antenna prototype including the feeding structure are illustrated in Fig. 6. The far field measurements of the antenna are conducted using a robot supported millimeter-wave test range [15], [16]. Fig. 9 shows the measured gain of the antenna prototype as a function of frequency. The maximum antenna gain is determined to 24.7 dBi at 149.8 GHz. Co- to cross-polarisation isolation can be improved by an anisotropic UC configuration, which is realized by an additional slice in the pixels as shown in Fig. 6. The orientation of the slice follows the individual requirement of the anisotropic tensor components to enhance the polarisation. From the numerical simulation the antenna

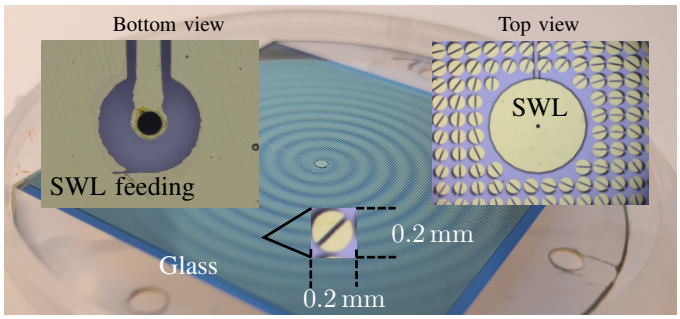

Fig. 6: Photograph of the realized holographic glass antenna prototype (inset shows the SWL).

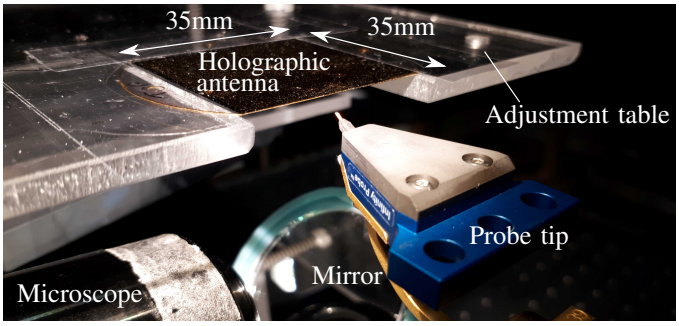

Fig. 7: Measurement setup for the holographic glass antenna prototype in upside down probing configuration.

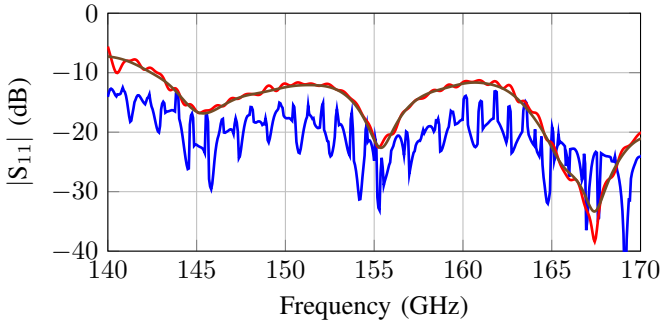

Fig. 8: Measured reflection coefficient of the realized glass antenna (— original data, — data w/o probe tips, — data w/o probe tips and spurious reflections of the env.).

provides a 3 dB-beam width of 4.8°, a sidelobe level of 18 dB, as depicted in Fig. 10a. The measured radiation pattern is illustrated in Fig. 10b for angles between −30° and 30°. A 3 dB-beam width of 4.7°, a sidelobe level of 15 dB, 24.7 dBi gain were measured. The measured reflection coefficient illustrated in Fig. 8 is below of −10 dB across the wide frequency range from 142 GHz. Additionally, the probe tip and spurious reflections from the environment have been removed by means of time domain filtering. The measured 3D-radiation pattern in Fig. 11 shows excellent side lobe suppression in all azimuth planes which coincides very good with the simulation results. The computed directivity from this measurement result is 26.2 dBi. A comparison to other state of the art AiP solutions is listed in Tab. I.

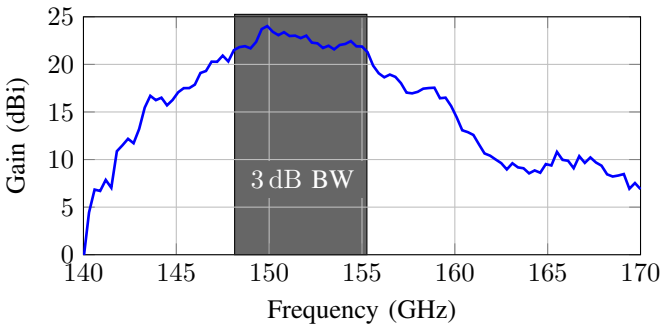

Fig. 9: Measured gain for the realized glass antenna.

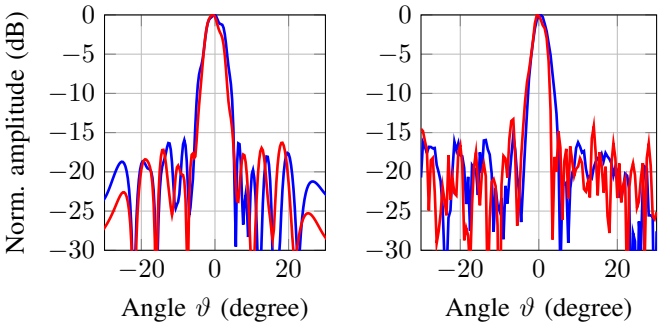

(a) Simulation (b) Measurement

Fig. 10: Radiation pattern of the anisotropic holographic glass antenna at 150 GHz (— Φ_0 = 0°, — Φ_0 = 90°).

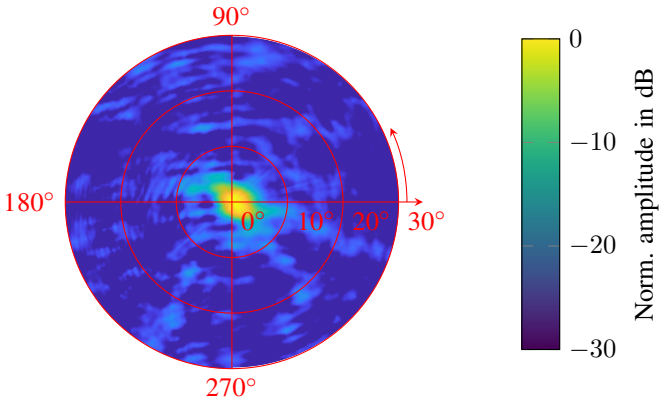

Fig. 11: Measured 3D-radiation pattern of anisotropic holographic glass antenna at 150 GHz.

TABLE I: Comparison to state of the art AiP solutions.

Literature	Gain (dBi)	f (GHz)	3 dB-BW (°)	SLL (dB)	size (mm ×mm)
this work	24.7	150	4.7	15	35×35
[17]	14.5	146	15	10	10×10
[18]	9	152	15	7	2.8×2.8
[19]	7.96	142	-	10	12×12
[20]	14	159	-	11	5×5

VII. Conclusion

In this paper a holographic glass antenna operating beyond 150 GHz for a hermetically sealed glass package in millimeter-wave sensor applications is presented. This has been verified by the realization and through characterization of the antenna element. The antenna prototype shows excellent agreement between the measured and simulated radiation pattern. The spherical radiation characteristics of the antenna up to elevation angles of 30° has been validated. The measured radiation patterns show a maximum antenna gain of 24.7 dBi, side lobe level of 15 dB, and a 3 dB-beam width of 4.7° which coincides with the simulation results. The novel aspects of glass with holographic antenna concept allows the realization of a large physical aperture using the package surface with low-cost material.

ACKNOWLEDGMENT

This work was funded by the VDI/VDE Innovation + Technik GmbH within the project GlaRA. – 16ES0692

REFERENCES

[1] M. Hitzler, P. Grüner, L. Boehm, W. Mayer, and C. Waldschmidt, "On monostatic and bistatic system concepts for mm-wave radar mmics," *IEEE Transactions on Microwave Theory and Techniques*, vol. 66, no. 9, pp. 4204–4215, 2018.

[2] A. Dürr, D. Schwarz, S. Häfner, M. Geiger, F. Roos, M. Hitzler, P. Hügler, R. Thomä, and C. Waldschmidt, "High-Resolution 160-GHz Imaging MIMO Radar Using MMICs With On-Chip Frequency Synthesizers," *IEEE Transactions on Microwave Theory and Techniques*, vol. 67, no. 9, pp. 3897–3907, Sep. 2019.

[3] T. Jaeschke, C. Bredendiek, and N. Pohl, "A 240 GHz ultra-wideband FMCW radar system with on-chip antennas for high resolution radar imaging," in *IEEE MTT-S International Microwave Symposium Digest (MTT)*, Jun. 2013, pp. 1–4.

[4] M. Hitzler, P. Grüner, L. Boehm, W. Mayer, and C. Waldschmidt, "On Monostatic and Bistatic System Concepts for mm-Wave Radar MMICs," *IEEE Transactions on Microwave Theory and Techniques*, vol. 66, no. 9, pp. 4204–4215, Sep. 2018.

[5] R. Feger, A. Hamidipour, and A. Stelzer, "Integrated mm-wave sensors in a package," in *2013 Asia-Pacific Microwave Conference Proceedings (APMC)*, 2013, pp. 209–211.

[6] B. Goettel, W. Winkler, A. Bhutani, F. Boes, M. Pauli, and T. Zwick, "Packaging Solution for a Millimeter-Wave System-on-Chip Radar," *IEEE Transactions on Components, Packaging and Manufacturing Technology*, vol. 8, no. 1, pp. 73–81, 2018.

[7] G. Minatti, F. Caminita, M. Casaletti, and S. Maci, "Spiral Leaky-Wave Antennas Based on Modulated Surface Impedance," *IEEE Transactions on Antennas and Propagation*, vol. 59, no. 12, pp. 4436–4444, Dec. 2011.

[8] G. Minatti, F. Caminita, E. Martini, M. Sabbadini, and S. Maci, "Synthesis of Modulated-Metasurface Antennas With Amplitude, Phase, and Polarization Control," *IEEE Transactions on Antennas and Propagation*, vol. 64, no. 9, pp. 3907–3919, Sep. 2016.

[9] T. Galler, T. Chaloun, K. Kröhnert, M. Schulz-Ruhtenberg, and C. Waldschmidt, "Hermetically Sealed Glass Package for Highly Integrated MMICs," in *49th European Microwave Conference (EuMC)*, 2019, pp. 292–295.

[10] HFSS version 19.2, Ansys Cooperation, Canonsburg, PA, USA, 2019.

[11] R. Ostholt, N. Ambrosius, D. Dunker, and J.-P. Delrue, "High-throughput via formation in solid-core glass for IC substrates," *MiNaPAD Conference, May 17-18,2017, Grenoble, France*.

[12] G. Minatti, M. Faenzi, E. Martini, F. Caminita, P. De Vita, D. González-Ovejero, M. Sabbadini, and S. Maci, "Modulated metasurface antennas for space: Synthesis, analysis and realizations," *IEEE Transactions on Antennas and Propagation*, vol. 63, no. 4, pp. 1288–1300, Apr. 2015.

[13] B. H. Fong, J. S. Colburn, J. J. Ottusch, J. L. Visher, and D. F. Sievenpiper, "Scalar and Tensor Holographic Artificial Impedance Surfaces," *IEEE Transactions on Antennas and Propagation*, vol. 58, no. 10, pp. 3212–3221, Oct. 2010.

[14] G. Goubau, "Surface Waves and Their Application to Transmission Lines," *Journal of Applied Physics*, vol. 21, no. 11, pp. 1119–1128, 1950. [Online]. Available: https://doi.org/10.1063/1.1699553

[15] L. Boehm, F. Boegelsack, M. Hitzler, and C. Waldschmidt, "The Challenges of Measuring Integrated Antennas at Millimeter-Wave Frequencies [measurements corner]," *IEEE Antennas and Propagation Magazine*, vol. 59, no. 4, pp. 84–92, Aug. 2017.

[16] ——, "Enhancements in mm-wave antenna measurements: automatic alignment and achievable accuracy," *IET Microwaves, Antennas Propagation*, vol. 11, no. 12, pp. 1676–1680, 2017.

[17] B. Zhang, C. Kärnfelt, H. Gulan, T. Zwick, and H. Zirath, "A D -Band Packaged Antenna on Organic Substrate With High Fault Tolerance for Mass Production," *IEEE Transactions on Components, Packaging and Manufacturing Technology*, vol. 6, no. 3, pp. 359–365, 2016.

[18] S. Beer, B. Göttel, C. Rusch, H. Gulan, and T. Zwick, "Off-chip antenna designs for fully integrated, low-cost millimeter-wave transceivers," in *2013 International Workshop on Antenna Technology (iWAT)*, 2013, pp. 199–202.

[19] C. Kärnfelt, B. Zhang, and H. Zirath, "A QFN packaged grid array antenna in low dielectric constant LTCC for D-band applications," in *2016 IEEE MTT-S International Microwave Workshop Series on Advanced Materials and Processes for RF and THz Applications (IMWS-AMP)*, 2016, pp. 1–4.

[20] B. Göttel, S. Beer, M. Pauli, and T. Zwick, "Ultra wideband D-band antenna integrated in a LTCC based QFN package using a flip-chip interconnect," in *2013 European Microwave Conference*, 2013, pp. 227–230.